



Article submitted to journal

Subject Areas:

biomathematics, computational
biology

Keywords:

contact network, diffusion process,
epidemiology, influenza,
mathematical model

Author for correspondence:

Md Shahzamal

e-mail:

md.shahzamal@students.mq.edu.au

Indirect interactions influence contact network structure and diffusion dynamics

Md Shahzamal^{1,2}, Raja Jurdak^{2,1}, Bernard Mans¹ and Frank de Hoog²

¹Department of Computing, Macquarie University, Sydney, Australia

²Data61, Commonwealth Scientific and Industrial Research

Organization (CSIRO), Australia

Interaction patterns at the individual level influence the behaviour of diffusion over contact networks. Most of the current diffusion models only consider direct interactions among individuals to build underlying infectious items transmission networks. However, delayed indirect interactions, where a susceptible individual interacts with infectious items after the infected individual has left the interaction space, can also cause transmission events. We define a diffusion model called the same place different time transmission (SPDT) based diffusion that considers transmission links for these indirect interactions. Our SPDT model changes the network dynamics where the connectivity among individuals varies with the decay rates of link infectivity. We investigate SPDT diffusion behaviours by simulating airborne disease spreading on data-driven contact networks. The SPDT model significantly increases diffusion dynamics (particularly for networks with low link densities where indirect interactions create new infection pathways) and is capable of producing realistic disease reproduction number. Our results show that the SPDT model is significantly more likely to lead to outbreaks compared to current diffusion models with direct interactions. We find that the diffusion dynamics with including indirect links are not reproducible by the current models, highlighting the importance of the indirect links for predicting outbreaks.

1. Introduction

Modelling diffusion processes on contact networks is an important research area for epidemiology, marketing, and cybersecurity. In the diffusion processes, contagious items initially appear at one or more nodes of interacting systems and then spread over the system through inter-node transmissions occurred due to interactions among nodes. Thus, a wide range of research has been conducted to understand the co-relations between diffusion dynamics and underlying contact network properties which are defined by interaction patterns [1–4]. Most diffusion models assume both infected and susceptible individuals are simultaneously present in the same physical space (e.g. visiting a location) or virtual space (e.g. friendship in online social networks) for an inter-node transmission, called individual-level transmission, to occur. We denote these models as same place same time transmission based diffusion (SPST diffusion) which only accounts for individual-level transmission links created by direct interactions to build underlying contact networks [5,6]. Examples of the SPST diffusion are

arXiv:1906.02405v1 [cs.SI] 6 Jun 2019

message dissemination in Mobile Ad-hoc Networks [7–9], information diffusion in online social networks [10] and infectious disease spreading through physical contacts [11].

The focus on concurrent presence (real or virtual), however, is not sufficiently representative of a class of diffusion scenarios where inter-node transmissions can occur via indirect interactions, i.e. where susceptible individuals receive contagious items even if the infected individuals have left the interaction location. For example, an individual infected by the airborne disease can release infectious particles in the air through coughing or sneezing. The particles are then suspended in the air so that a susceptible individual arriving after the departure of the infected individual can still get infected [5,12,13]. Similarly, a piece of information posted by an existing member in an online social blog can be seen by a newly joined member, even though the new member was not present when the piece of information was posted [14,15]. Queen message dissemination in the social ant colonies and pollen dissemination in the ecology also follow a similar mechanism [16]. In these scenarios, current diffusion models can miss significant transmission events during delayed indirect interactions.

We develop a diffusion model to capture individual-level transmission links created for both the direct interactions where susceptible and infected individuals are present at visited locations and indirect interactions where susceptible individuals are present or arrive after the infected individuals have left the locations. We call this model same place different time transmission based diffusion (SPDT diffusion). In this model, links are created through location and time and called SPDT links. The SPDT model captures transmission events occurring simultaneously at multiple locations by an infected individual (transmission at the current location due to the direct interaction, and transmissions at the previous locations due to indirect interactions). In this diffusion model, the link infectivity, probability of causing infection by an SPDT link which is created for direct and/or indirect interactions, depends on various factors such as the presence of infected and susceptible individuals at the interaction location, decay rates of infectious items and environmental conditions etc [5,12,17,18]. The current SPST models cannot account these features introduced due to the inclusion of indirect interactions with diffusion processes.

The SPDT diffusion model is integrated with a new assessment method for finding SPDT link infectivity. For an airborne disease, this involves two steps: 1) determining the number of infectious particles inhaled by the susceptible individual (intake dose) and 2) analytically finding the corresponding infection risk, probability of contracting disease. To assess the infection transmission probability of an interaction between susceptible and infected individuals in airborne disease, the Wells-Riley model and its variants are widely used [12,17,19]. These models can determine infection probability for a susceptible individual who is exposed to infectious particles generated by a number of infected individuals for a period of time at a visited location. They account the particle generation rates of infected individuals, the breathing rate of the susceptible individual and particle removal rates from the interaction location. However, these models do not support link infectivity assessment for the SPDT model as they do not consider arrival and departure times of individuals at interaction locations. Thus, they can not account transmission occurred during indirect interactions. Our proposed SPDT link infectivity assessment method is based on the Wells-Riley model yet it accounts for transmissions during indirect interactions among susceptible and infected individuals as well as the impacts of environmental and structural factors of interaction locations through particles decay rates.

The diffusion behaviours of our proposed SPDT model are explored through simulating airborne disease spreading on empirical dynamic contact networks constructed from location updates of a social networking application called Momo [20]. In these networks, the disease transmission links are created for both direct and indirect co-located interactions. We analyze 56 million location updates from 0.6 million Momo users of Beijing city to extract all possible direct and indirect links. This yields a SPDT contact network (SDT) of 364K users and exclusion of indirect links from the above process provides a SPST contact network (SST) of the same users. These networks are based on the sparse data as users were not regular in using Momo App. Thus, the impact of indirect interactions can be stronger with denser data which is explored by building denser networks (DDT and DST) from the SDT network. For the inclusion of indirect interactions, the SPDT model adds new transmission links and new users to the SPDT networks over the SPST networks. To understand the enhancement in diffusion behaviours for these additions, another SPDT and SPST networks (LDT and LST) are built with the same users and same link densities of DDT network. We adopt a generic Susceptible-Infected-Recovered (SIR) epidemic model to simulate airborne disease spreading on these networks [21].

The SPDT model alters the underlying contact network dynamics (e.g. contact frequency and contact duration for adding new indirect links) which also vary with the infectivity decay rates of SPDT links. This variation in the underlying connectivity affects the diffusion dynamics [22,23]. The infectivity decay rates of SPDT links are strongly influenced by the infectious particle decay rates at the interaction locations. Therefore, we first investigate how various particle decay rates change the underlying connectivity of SPDT model and hence diffusion dynamics, using known airborne disease parameters such as infectiousness of particles and infectious period of a disease [4,24–27]. We also

study how the impacts of particle decay rates vary with biological disease parameters. Then, we compare the SPDT diffusion dynamics with SPST diffusion dynamics to identify novel behaviours that the SPDT model introduces. Finally, we show that the SPDT diffusion dynamics cannot be reproduced by current SPST models, even when controlling for link densities, and this characterizes the limitations of the underlying network connectivity in the SPST model compared to that of the SPDT model.

2. SPDT diffusion model

The infectious items transmission network in the SPDT model is built at the individual-level with direct and (delayed) indirect transmission links created for direct and indirect interactions. The link creation procedure for this model can be explained by airborne disease spreading phenomena as shown in Fig. 1. In this particular scenario, an infected individual A (host individual), red circle, arrives at location L at time t_1 followed by the arrival of susceptible individuals u and v, green circles, at time t_2 . The appearance of v at L creates a directed link for transmitting infectious particles from A to v and lasts until time t_4 making direct link during $[t_2, t_3]$ and indirect link during $[t_3, t_4]$. The indirect link is created as the impact of A still persists (as the virtual presence of A is shown by the dashed circle surrounding A) after it left L at time t_3 , due to the survival of the airborne infectious particles in the air of L. But, the appearance of u has only created direct links from A to u during $[t_2, t_3]$. Another susceptible individual w arrives at location L at time t_5 and a link is created from A to w through the indirect interaction due to A's infectious particles still being active at L. However, the time difference between t_5 (arrival time of w) and t_4 (departure time of A) should be the maximum δ such that a significant particles concentration is still present at L after A left at t_4 .

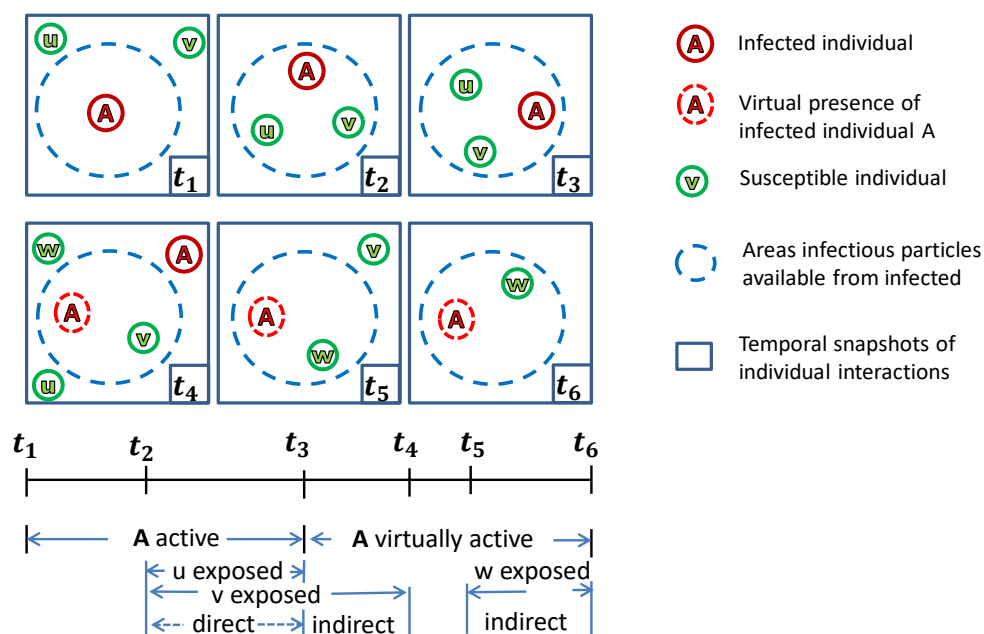


Figure 1. Disease transmission links creation for co-located interactions among individuals in SPDT model. The upper part shows the six snapshots of interactions over time and the lower part shows the periods of exposure through direct and indirect interactions. Susceptible individuals are linked with the infected individual if they enter the blue dashed circle areas within which infectious particles are available to cause infection

The infected individual makes several such visits, termed as active visits, to different locations and transmits disease to susceptible individuals through his infectious particles. The unique feature of the SPDT model comparing to SPST models is that infected individual can transmit disease at multiple locations in parallel due to direct transmission links at current locations and indirect transmission links at the previous locations that do not require the presence of host individual. However, visits of infected individuals at locations where no susceptible individuals are present or susceptible individuals visit after the time period δ do not lead to disease transmissions. During the active visits, directed transmission links between infected individuals and susceptible individuals are created through location and time. We call these links SPDT links which can have components: direct transmission links and/or indirect transmission links. The disease transmission probability over a SPDT link is influenced by the indirect link duration

along with direct link duration, the time delay between neighbour and host individual appearances at the interaction location and decay rates of infectious particles from the location [5,12,17].

We integrate a method with the SPDT model to assess the probability of contrasting disease for an SPDT link (SPDT link infectivity) using generic assumptions. This method captures the parallel disease transmission events of infected individuals. Suppose that an infected individual A appears at a location L at time t_s and deposits airborne infectious particles into the proximity with a rate g (particles/s) until he has left the location at t_l . These particles are homogeneously distributed into the air volume V of proximity and the particle concentration keeps increasing until it reaches a steady state. Simultaneously, active particles decay at a rate r (proportion/s) from the proximity due to various reduction processes such as air conditioning, settling down of particles to the ground and losing infectivity.

Thus, the particle concentration C_t at time t after the infected individual A arrives at L is given by [17,28]

$$C_t = \frac{g}{rV} \left(1 - e^{-r(t-t_s)}\right) \quad (2.1)$$

If a susceptible individual u (as Fig. 1) arrives at location L at time $t'_s \geq t_s$ and continues staying with A up to $t'_l < t_l$, the number of particles E_d inhaled by u through this direct link is

$$E_d = \frac{gp}{rV} \left[t'_l - t'_s + \frac{1}{r} e^{-r(t'_l-t_s)} - \frac{1}{r} e^{-r(t'_s-t_s)} \right] \quad (2.2)$$

where p is the pulmonary rate of u. If a susceptible individual v (as Fig. 1) stays with A as well as after A leaves L at t_l where ($t'_l \geq t_l$), it will have both direct and indirect links. The value of E_d for v within the time t'_s and t_l is given by

$$E_d = \frac{gp}{rV} \left[t_l - t'_s + \frac{1}{r} e^{-r(t_l-t_s)} - \frac{1}{r} e^{-r(t'_s-t_s)} \right] \quad (2.3)$$

For the indirect link from time t_l to t'_l , we need to compute the particle concentration during this period which decreases after A leaves at t_l . The particle concentration at time t is given by

$$C_t = \frac{g}{rV} \left(1 - e^{-r(t_l-t_s)}\right) e^{-r(t-t_l)} \quad (2.4)$$

The individual v inhales particles E_i during the indirect period from t_l to t'_l is

$$E_i = \frac{gp}{Vr^2} \left(1 - e^{-r(t_l-t_s)}\right) \left[1 - e^{-r(t'_l-t_l)}\right] \quad (2.5)$$

If a susceptible individual w is only present for the indirect period at the proximity (as Fig. 1), the number of inhaled particles for the indirect period from t'_s to t'_l is given by

$$E_i = \frac{gp}{Vr^2} \left(1 - e^{-r(t_l-t_s)}\right) \left[e^{-r(t'_s-t_l)} - e^{-r(t'_l-t_l)}\right] \quad (2.6)$$

Therefore, total inhaled particles through an SPDT links can be written as

$$E_l = \frac{gp}{Vr^2} \left[r(t_i - t'_s) + e^{rt_l} \left(e^{-rt_i} - e^{-rt'_l} \right) \right] + \frac{gp}{Vr^2} \left[e^{rt_s} \left(e^{-rt'_l} - e^{-rt'_s} \right) \right] \quad (2.7)$$

where t_i is given as follows: $t_i = t'_l$ when SPDT link has only direct component, $t_i = t_l$ if SPDT link has both direct and indirect components, and otherwise $t_i = t'_s$. If $t_s < t'_s$, we have to set $t_s = t'_s$ for appropriate exposure. If a susceptible individual receives m SPDT links from infected individuals during an observation period, the total exposure E is

$$E = \sum_{k=0}^m E_l^k \quad (2.8)$$

where E_l^k is the received exposure for k^{th} link. The probability of the infection spreading can be determined by the dose-response relationship defined as

$$P_I = 1 - e^{-\sigma E} \quad (2.9)$$

where σ is the infectiousness of virus to cause infection [5,29,30]. This value depends on both disease and virus types.

3. Data and Methods

3.1 Data set

This study exploits location update information collected from users of a social discovery network *Momo*¹. The Momo App updates the current user locations to the Momo server while the App is used. The authors of [20] collected location updates from the server every 15 minutes over 71 days (from May to October 2012). Each database entry includes coordinates of the location, time of update and user ID. The App updates a user's location whenever the user moves at least 10m. For this study, the updates from Beijing are used as it is the city with the highest number of updates for the period of 32 days from 17 September, 2012 to 19 October, 2012. This data contains almost 56 million location updates from 0.6 million users.

3.2 Contact networks

A data-driven individual dynamic contact network is built analyzing location updates of Momo users collected from Beijing city over 32 days. This network includes possible direct and indirect transmission links due to direct and indirect co-location interactions among users. To create an SPDT link between a host user (assumed infected with an airborne disease) and a neighbouring user (assumed susceptible - not infected yet), the neighbour user should make location updates within 20 meters distance of host user's current locations and updates must be made within 200 minutes of the last update of the host user from the current location. When the host user's last update is more than 20 metres distance of the first update of the current location or after 30 minutes of his the last update, the new link creation process is started at the new location. However, link creation is continued at the previous location up to 200 minutes of last update. If a user does not have any neighbour user over the observation period, he/she is not included in the constructed network. Therefore, the processing of 56 million location updates from 0.6 million users yields a SPDT contact network of 364K users with a total of 6.86 million links. To compare SPDT diffusion against SPST diffusion, we generate a corresponding SPST network excluding the indirect links from the SPDT network.

The above constructed networks show low link densities as users often appear in the system for an average of 3-4 days and then disappear for the remainder of the data collection period. This is characterised by the limitations of the collection system and user's behaviours when using the social networking App. Thus, these networks are called Sparse SPDT network and Sparse SPST network (denoted as SDT network and SST network in the rest of the paper) which capture partial snapshots of real-world social contact networks. Therefore, these sparse networks might underestimate the diffusion dynamics because infected individuals may not be present in the network for all of their infectious periods and miss some disease transmission events. This may also lead to a wrong conclusion regarding the contribution of SPDT diffusion model. To understand the SPDT diffusion in networks with high link densities, we reconstruct a Dense SPDT network (DDT network) repeating links from available days of a user to the missing days for that user [2,3]. Then, the corresponding Dense SPST network (DST network) is built excluding indirect links from the DDT network.

The users who are only connected with other users through indirect links in the above SPDT networks become isolated in SPST networks as indirect links do not exist in SPST networks. Thus, link densities reduce in SPST networks compared to the corresponding SPDT networks. Moreover, the underlying social contact structures are also reshaped since some users disconnect from each other. This is the inherent property of SPDT model over SPST model and its impacts on diffusion dynamics are characterised as follows. We create two networks, LDT and LST, which maintain the same link densities and the same underlying social structure as that of the DDT network. In this format, neighbouring user's arrival time t'_s of the SPDT links that have only indirect components in DDT network is set to the t_s of the host user to obtain a LDT network. Then, indirect components of links are removed from the LDT network to build the LST network which now has the same link density and no isolated users. These two networks are used to identify the novel diffusion behaviours of SPDT model comparing to SPST model while varying link densities and underlying social structures. All SPDT networks assume the same network structure (same clustering coefficient and degree distribution) than the SDT network, similarly all SPST networks structures are the same as the SST network.

3.3 Epidemic Model

A generic Susceptible-Infected-Recovered (SIR) epidemic model is adapted to emulate airborne disease propagation on the constructed contact networks [21]. Individuals are in one of the three states: susceptible, infectious and recovered. If an individual in the susceptible state receives SPDT links from infected individuals, they may move to the infectious

¹<https://www.immomo.com>

state with the probability derived by Eqn. 2.9. Then, the infectious individual continues to produce infectious particles over its infectious period τ days until they enter the recovered state. In this epidemic model, no event of births, deaths or entry of new individual are considered.

3.4 Simulation setup

The simulations are step forwarded in our experiments with one day interval. The authors of [2,3] have studied that aggregating contact information in one day provides similar disease spreading dynamics of considering each contact separately. Moreover, newly infected individuals in an influenza-like disease have an incubation period before becoming infectious [4]. Thus, the one day interval can be considered as a latent period. All simulations are run for a period of 32 days. Simulations from a single seed node, initially infected, requires a long time to produce a full epidemic curve (disease prevalence reaches to a peak value and then declines). Thus, we chose an initial set of 500 seed nodes randomly in each experiment to start simulations assuming that it will be capable to show the full epidemic curve in 32 days. In addition, it will sufficiently demonstrate the contribution of indirect links within this setting. During each day of disease simulation, the received SPDT links for each susceptible individual from infected individuals are separated and infection causing probabilities are calculated by Eqn. 2.9. The volume V of proximity in Eqn. 2.7 is fixed to 2512 m^3 assuming that the distance, within which a susceptible individual can inhale the infectious particles from an infected individual, is 20m and the particles will be available up to the height of 2m [5,31]. The other parameters are assigned as follows: particle generation rate $g = 0.304$ PFU (plaque-forming unit)/s and pulmonary rate $q = 7.5$ liter/min [26, 27,31]. Based on the air exchange rates $0.5\text{-}6\text{h}^{-1}$ in public settings [32,33], infectivity decay rate of generated particles and settling rates [5], we assume particles removal rates are in the range $0.2\text{-}8\text{h}^{-1}$. Therefore, particles may require 7.5 min to 300 min to be removed from interaction areas after their generation. We assign $r = \frac{1}{60b}$ to Eqn 2.7 where b is particle removal time randomly chosen from [7.5-300] min given a median particle removal time r_t . The particle removal rates r in our experiments are discussed with r_t , i.e. particle decay rates r_t mean the corresponding particle removal rates r drawn from the above process for all SPDT links and r_t is median of $1/60r$. The parameter σ is set to 0.33 as the median value of required exposures for influenza to induce disease in 50% susceptible individuals is 2.1 PFU [25]. Susceptible individuals stochastically switch to the infected states in the next day of simulation according to the Bernoulli process with the infection probability P_I (Eqn 2.9). Individual stays infected up to τ days randomly picked up from 3-5 days maintaining $\bar{\tau} = 3$ days (except when other ranges are mentioned explicitly) [4].

3.5 Characterizing metrics

The daily simulation outcomes are obtained for the following parameters: number of infections I_n caused at a simulation day, number of infected individuals recovered from infection and current number of infected individuals I_p (disease prevalence) in the system on a simulation day. For characterising the diffusion dynamics, we find the disease reproduction abilities of infected individuals in a network as follows. The disease prevalence dynamics at time t in the compartmental model is given by

$$\frac{dI_p(t)}{dt} = (\beta S(t) - \sigma) I_p(t) \quad (3.1)$$

where β is the infection rate, σ is the recovery rate, $S(t)$ is the number of susceptible individuals at t [34]. If $\beta S(t) > \sigma$, the disease prevalence $I_p(t)$ gets stronger at time t . Otherwise, $I_p(t)$ reduces and continuous reduction dies out the disease. The ratio $\beta S(t)/\sigma$ is called effective reproduction number, the number of secondary infections caused by an infected individual based on the condition that all individuals in the network are not susceptible to the disease, and termed as R_t . Therefore,

$$R_t = \frac{\beta S(t)}{\sigma} = \frac{\beta S(t) I_p(t)}{\sigma I_p(t)} = \frac{I_n(t)}{I_r(t)}$$

We can replace $\beta S(t) I_p(t)$ with the number of infections I_n caused on a simulation day and $\sigma I_p(t)$ with the number of recovered individual from infection $I_r(t)$. Thus, we can estimate the effective reproduction number R_t at each simulation day using I_n and I_r . Then, we take the average R_e of R_t as the overall strength of a disease to diffuse on the contact networks.

4. Results and analysis

The inclusion of indirect transmission links makes the underlying transmission network of SPDT model strongly connected compared to the SPST model. Individuals who are not connected in the SPST model may get connected

in the SPDT model for adding indirect transmission links. Hence, the underlying connectivity becomes denser in the SPDT model. Secondly, the number of links between two connected individuals may increase with the inclusion of indirect links. Besides, a direct link connecting two individuals in SPST models can be extended by appending an indirect transmission link in the SPDT model. These enhancements increase the disease transmission probabilities among individuals in the SPDT model. Therefore, the diffusion dynamics will be amplified in the SPDT model compared to the SPST model [23,35].

The SPDT model alters the network connectivity when changing the particle decay rates r_t which influences the diffusion dynamics. To understand this, we consider Fig. 2 where the particle concentration rises and falls for various r_t according to Eqn. 2.1 and Eqn. 2.4 at a location visited by an infected individual. Here, the particle concentration decays are estimated assuming that the infected individual has stayed in the visited location for 200 min. As the value of r_t is increased, significant particle concentration is available for longer time at the interaction location (Fig. 2B). This allows more neighbouring individuals to receive exposure when visiting locations within the longer period δ at higher r_t , when indirect transmission links can be created. Therefore, the underlying network connectivity becomes denser with increasing r_t . In addition, the exposure through direct and indirect links become stronger as r_t increases (Fig. 2A and Fig. 2B). Thus, individuals in the SPDT model get connected more strongly at high r_t and link infectivity increases. We, therefore, study the variations in the underlying network connectivity with r_t and their impacts on the diffusion dynamics.

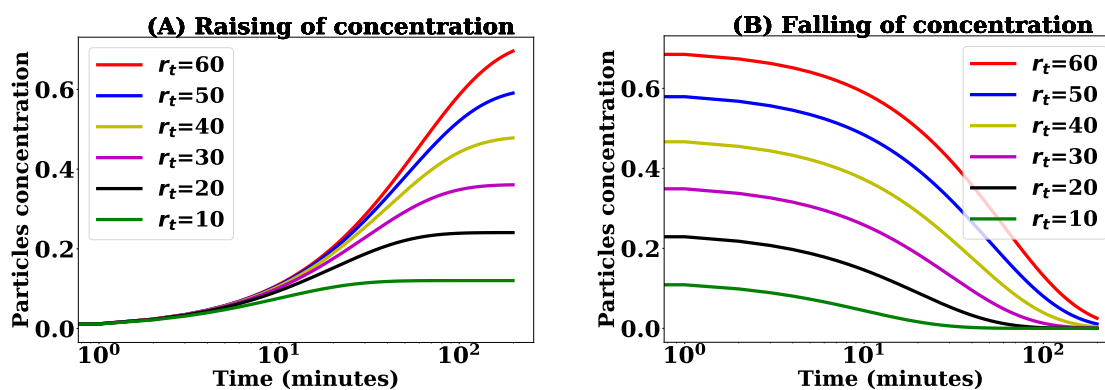


Figure 2. Particles concentrations for various particles decay rates r_t at a visited location when A) an infected individual is present at the location over 200 min and B) the infected individual has left the location after staying 200 min

The disease parameters are known to influence the spreading dynamics as well [24]. In our SPDT model definition, we find the interaction between the infectiousness of diseases and the particle decay rates (Eqn 2.9). For example, the higher value of infectiousness σ will increase the infection risk of SPDT links. Thus, the required threshold of the particle concentration to cause infection through a SPDT link reduces and the indirect link creation window δ will be longer. This means that more susceptible individuals will create links with the infected individual for visiting the same location at a higher σ . Therefore, the underlying connectivity gets stronger with high σ for a given particle decay rates r_t . In addition, the other disease parameter, the infectious period τ , also affects disease spreading varying the recovery rates of infected individuals. Thus, our last experiment studies how the SPDT model behaves with stronger disease parameters and various r_t , while the number of individuals with high degree increases compared to those of the SPST network (Fig. 3A). The same changes are found for the clustering coefficient as well (Fig. 3B).

4.1 Network analysis

We analyze the enhancements in the underlying connectivity of the SPDT model exploring two network metrics: degree centrality and local clustering coefficient. We study the metrics for static and dynamic representations of sparse networks (SST and SDT networks) over 32 days. In static networks, an edge between two individuals is created once they have a link over 32 days. A SPDT link will be an edge when the inhaled exposure E_l by the susceptible individual is $E_l \geq 0.01$ particles (as Eqn.2.9 shows P_l negligible at $E_l = 0.01$). However, the edges are not weighted by E_l or the number of SPDT links. We set r in Eqn.2.7 corresponding to $r_t = 60$ min to understand the maximum enhancements by the SPDT model. We find the degree distribution, the number of neighbours a host individual has contacted, and the local clustering coefficient, which is the ratio of the number of triangles present among the neighbours and the possible maximum triangles among neighbours. To compute the clustering coefficient, we neglect the directions of links as our

focus is to understand the changes in connectivity. The results are obtained using NetworkX [36] and are shown in Fig. 3A and Fig. 3B for the static network. In the SPDT network, the number of individuals with low degree decreases while the number of individuals with high degree increases compared to those of the SPST network (Fig. 3A). The same changes are found for the clustering coefficient as well (Fig. 3B).

The dynamic representations are created by aggregating networks over each day where an edge between two individuals is created once they have a link on that particular day. Then, we measure the daily average degree and clustering coefficient for the SDT network with the values of $r_t = \{10, 20, 30, 40, 50, 60\}$ min and also for the SST network. The results are shown in Fig. 3C and Fig. 3D. The daily average individual degree and average clustering coefficient in the SPDT model are significantly larger than that in the SPST model and the difference increases as r_t increases. However, the increases in daily average degree and daily average clustering coefficient decrease at the higher values of r_t as the particle concentration reaches a steady state quickly at high r_t . Both the static and dynamic networks show the stronger connectivity in the SPDT model than the SPST model and the network properties vary with particle decay rates r_t .

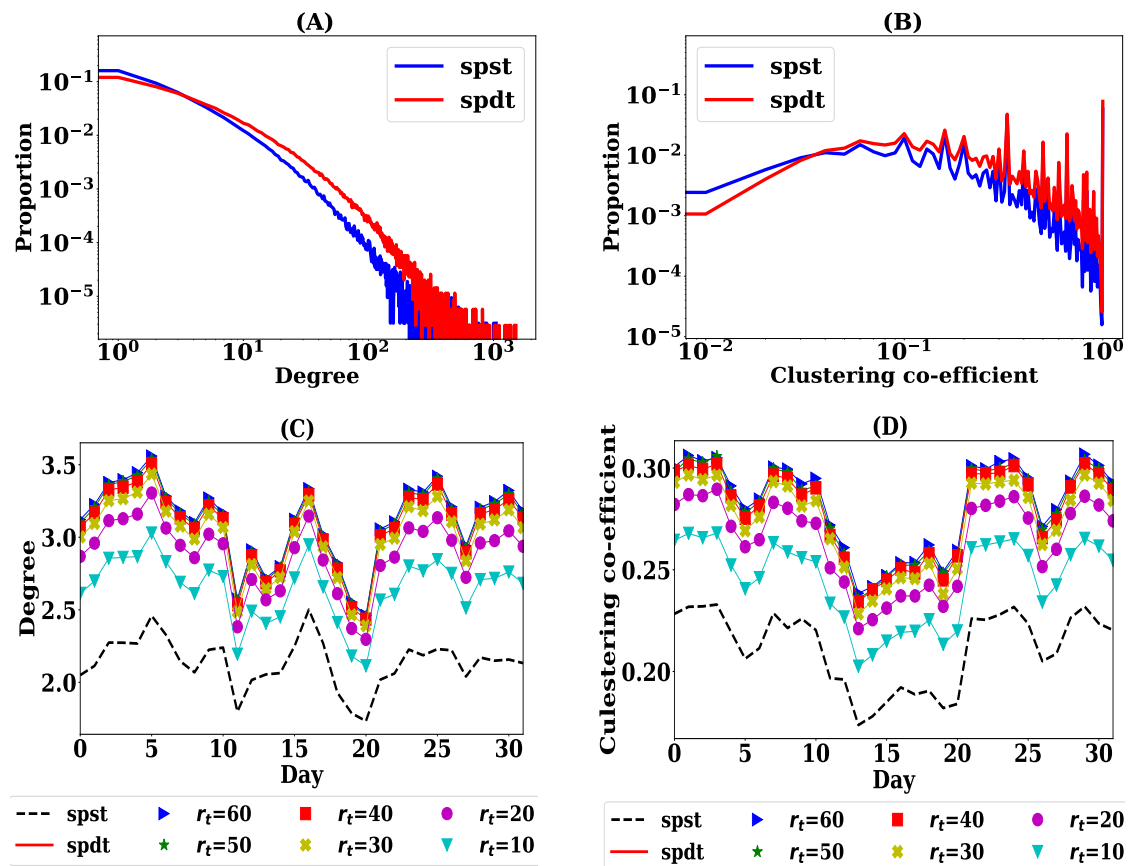


Figure 3. Comparing SPST and SPDT networks properties: A) degree distribution in static networks, B) clustering co-efficient distribution in static networks, C) daily average degree in dynamic networks, and D) daily average clustering co-efficient in dynamic networks

4.2 Diffusion for various particle decay rates

This experiment explores the influence of particle decay rates on diffusion dynamics varying r_t in the range [10, 60] minutes with a step of 5 minutes. We run 1000 simulations for each r_t on both SPDT and SPST networks with sparse and dense configurations. Fig. 4 shows the overall diffusion characteristics for all r_t where y-axes shows the impacts on diffusion dynamics for corresponding r_t . In total, outbreak sizes (total infections caused over the simulation period) in the SPDT model increase linearly with r_t (Fig. 4A). The amplification with the SPDT model is up to 5.6 times for sparse networks and 4.3 times for dense networks at $r_t = 60$ min (Fig. 4B). The individuals in the SPDT model achieve strong disease reproduction abilities R_e relative to SPST (Fig. 4C). Thus, outbreak sizes are amplified in the SPDT model. The initial disease reproduction abilities (Fig. 4D), which is calculated at the first simulation day, shows how

the contact networks become favourable for diffusion with increasing r_t in both SPDT and SPST models. The initial disease reproduction abilities in SPDT model are strongly influenced by r_t .

The temporal variation of disease prevalence for $r_t = \{15, 30, 45, 60\}$ min are presented in Fig. 5 while Fig. 6 shows the variations in disease reproduction rates R_t . The results show that the diffusion dynamics are strongly governed by r_t . The SDT network shows growing of disease prevalence I_p from the initial 500 infected individuals for values of $r_t \geq 45$ min while I_p drops for all other values (Fig. 5B). In the heterogeneous contact networks, the disease gradually reaches to the individuals, called higher degree individuals, who have high contact rates and hence the value of R_t gradually increases [35,37]. This growth of R_t is faster at high r_t due to strong underlying connectivity (Fig. 6B). However, individuals with a high degree get infected earlier and the number of susceptible individuals reduces through time. Hence, an infection resistance force grows in the network and the rate R_t of infected individuals decreases. Therefore, an initial small R_t for $r_t \geq 45$ min quickly increases above one which grows I_p as long as R_t remains above one and then decreases (Fig. 6B). For $r_t < 45$ min, R_t slowly grows above one due to the weak underlying network connectivity with low r_t and I_p decreases significantly with time. As a result, I_p increases slightly and then start dropping. In the SST network, I_p could not grow for any value of r_t due to very small initial R_t and lack of connectivity for considering only direct links (Fig. 5A and Fig. 6A). The SDT network at $r_t = 10$ min shows similar trend that is for the SST network (Fig. 6A and Fig. 6B). This is because the SDT network becomes similar to the SST network due to weak underlying connectivity at this low r_t where creations of indirect links are limited.

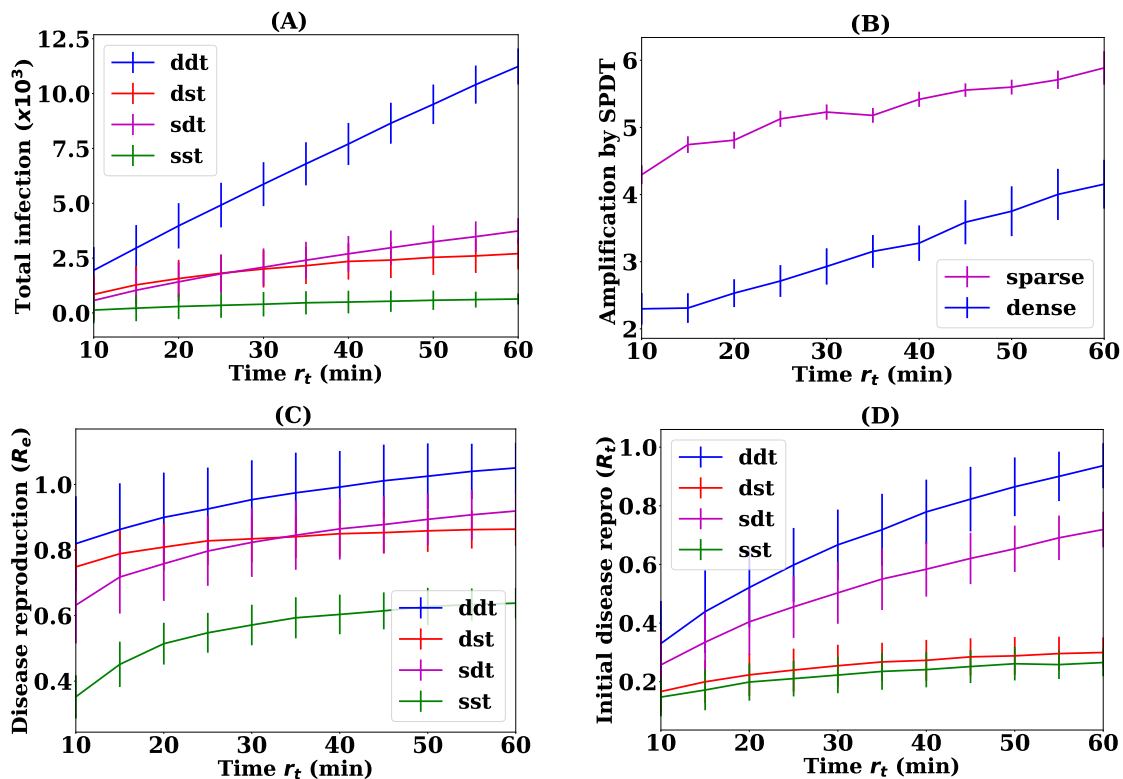


Figure 4. Diffusion dynamics including interquartile ranges on SPST and SPDT networks with particles decay rates r_t : A) total number of infections - outbreak sizes, B) amplification by SPDT model, C) effective disease reproduction number R_e , and D) initial disease reproduction number R_t

The impact of SPDT model becomes stronger in the dense DDT network: infected individuals apply their full infection potential by being every day in the network. The total infections (outbreak sizes) and the disease prevalence I_p increase significantly (Fig. 4A and Fig. 5D). The DDT network is capable of increasing I_p even at lower $r_t \geq 20$ min. Due to high link density, the disease reproduction rate R_t in the DDT network reaches one quickly and then increases faster as time goes (Fig. 6D). The rate R_t has multiple effects on the disease prevalence I_p . For the higher value of I_p and $R > 1$, small changes in R_t have a large increase in I_p . Small variations in r_t change R_t which in turn significantly changes I_p in the DDT network. Conversely, I_p first drops for all values of r_t in the DST network and then start increasing after some days as high degree individuals are infected. However, this increase is not within the same range than the DDT network due to a weak R_t and a lack of underlying connectivity. Similarly, the DDT network with low $r_t < 20$ min behaves comparatively to the DST network as the underlying connectivity becomes weak.

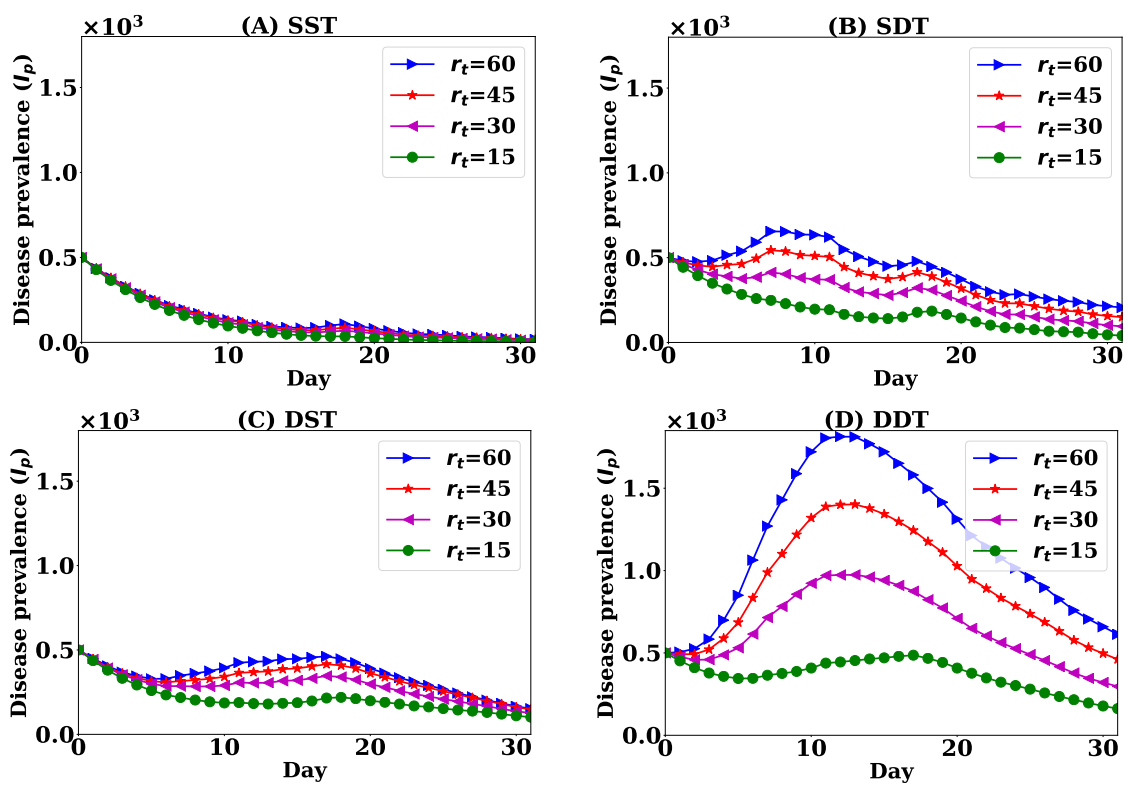


Figure 5. Disease prevalence, current number of infected individual in the network, dynamics over simulation days for SPDT and SPST models with various particles decay rates r_t : A) sparse SPST network (SST), B) sparse SPDT network (SDT), C) dense SPST network (DST), and D) dense SPDT network (DDT)

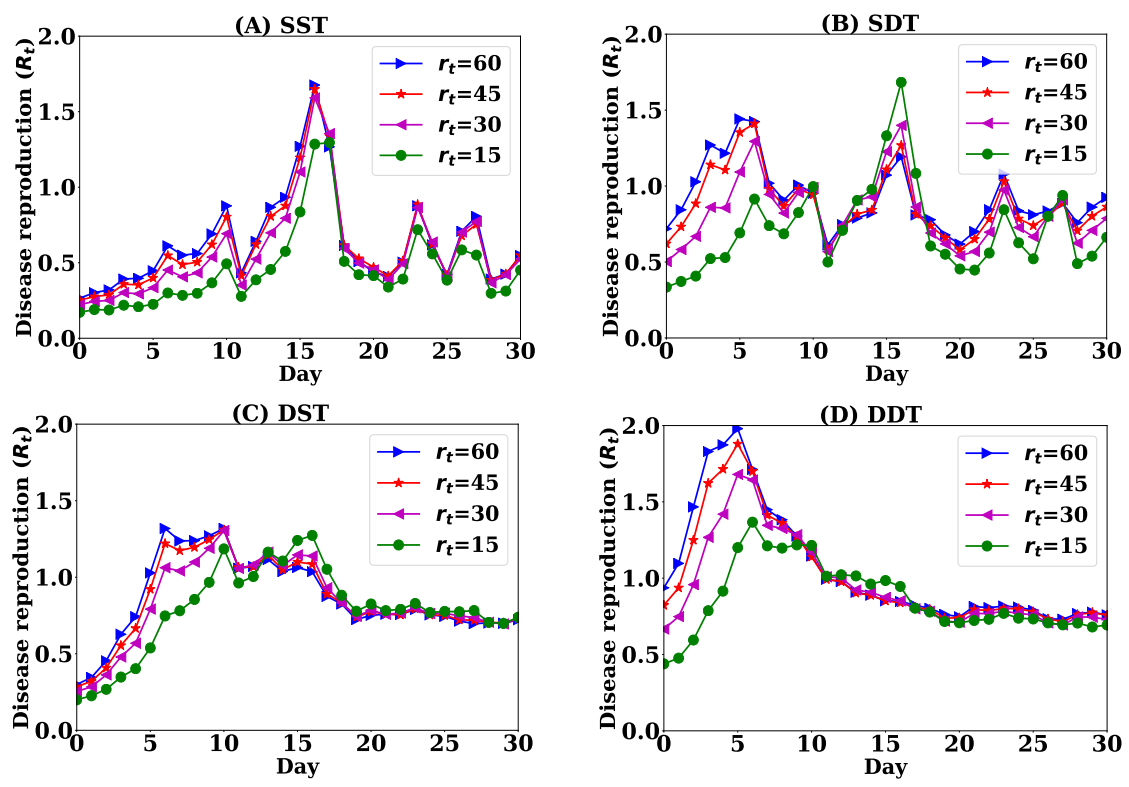


Figure 6. Daily variations in disease reproduction rate R_t with particle decay rates r_t : A) sparse SPST network (SST), B) sparse SPDT network (SDT), C) dense SPST network (DST), and D) dense SPDT network (DDT)

4.3 Diffusion for various disease parameters

The impact of particle decay rates r_t on SPDT diffusion dynamic increases with increasing infectiousness σ . For analysing this, we run simulations for $\sigma = \{0.33, 0.4, 0.5\}$ on both SPST and SPDT networks with varying r_t . The results are presented in Fig. 7A and Fig. 7B. The amplification by SPDT model increases as σ increases (Fig. 7A). The required r_t to grow the disease prevalence I_p in SPDT model reduces with increasing σ [38]. Besides, we notice that SPDT model makes a longer linear amplification (continuous growth of infection amplification with increasing r_t , which should stop at some value of r_t) in dense networks. Except for DDT network, the growth in the total infection gain at low r_t due to an increase in σ is higher compared to that at high r_t . This is shown in the Fig. 7B through the ratios of total infections at $r_t = 60$ min and $r_t = 10$ min. However, the DDT network shows a different behaviour as the growth in total infection gain at high r_t still increases with σ increases. Having higher link density and more high degree individuals, the DDT network can achieve a stronger infection force at high r_t to override the infection resistance force coming from the reduction in susceptible individuals. However, the other three networks are affected by the infection resistance force at high r_t more strongly than the low r_t as they have lack of underlying connectivity (the sparse SST and DST networks only account indirect links and SDT has low link density).

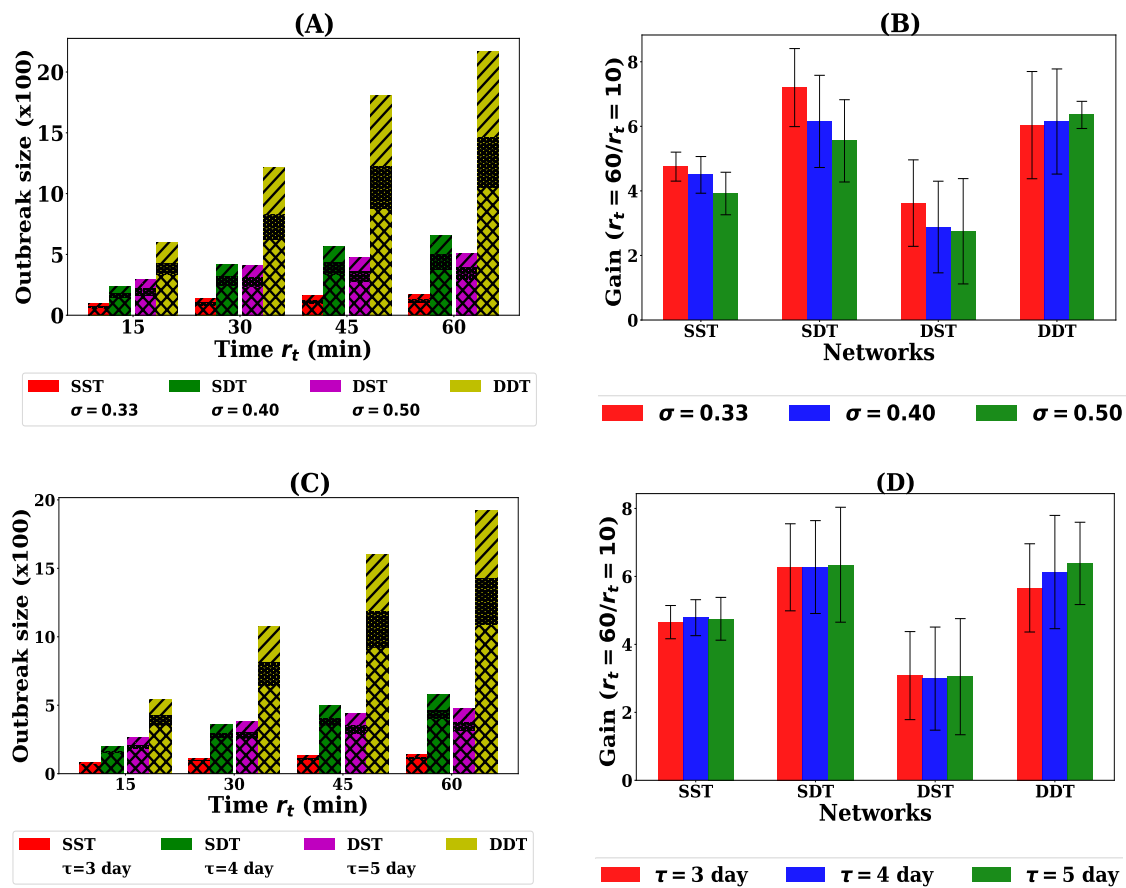


Figure 7. Diffusion dynamics for various disease parameters in the different networks: A) outbreak sizes for various infectiousness σ - different pattern showing amplification for increasing σ , B) gains in outbreak sizes for changing r_t from 10 min to 60 min for various σ , C) outbreak sizes for various infectious period τ - different pattern showing amplification for increasing τ , and D) gains in outbreak sizes for changing r_t from 10 min to 60 min for various τ

A longer infectious period τ also increases the disease reproduction ability R_t of infected individuals as recovery forces from infection are reduced. The diffusion behaviours for $\bar{\tau} = \{3, 4, 5\}$ days with constant $\sigma = 0.33$ are shown in Fig. 7. This also increases total infection (Fig. 7C) and reduces r_t to grow disease prevalence I_p [38]. In this case, the DDT network supports longer linear amplification as well while for other networks it reaches a steady state. Besides, the delays to reach a peak I_p become longer as $\bar{\tau}$ increases. This is because R_t is maintained over one for longer which grows I_p for longer [38]. As a result, the disease persists within the population for a longer time in SPDT model than SPST model.

5. Discussion

5.1 Diffusion on dynamic networks

Current diffusion models only consider concurrent interactions as a cause of individual-level transmission. However, there are several real scenarios where indirect delayed interactions can also cause transmission of infectious items and many infectious diseases spread this way [5,16,39,40]. Similar diffusion mechanisms occur for the dissemination of messages in social media and in ant colonies [14,16]. The importance of indirect transmission is studied in several infectious disease spreading models [30,41–43]. However, they did not account for the individual-level indirect transmissions in developing disease outbreaks. For airborne diseases, suspension of particles in the air and their risk to transmit disease are widely discussed, but how this suspension can contribute in diffusion dynamics within a population remains under-explored [12,19].

In our study, we have introduced a SPDT diffusion model accounting for the indirect transmissions along with the direct transmissions. Inclusion of indirect transmissions changes the network topology: 1) strengthening the existing direct links by appending indirect links and 2) connecting individuals who are not connected with the direct links. Therefore, the underlying connectivity gets denser and stronger in the SPDT model comparing to SPST model and diffusion dynamics are amplified. However, the enhancement of SPDT diffusion is varied with particle decay rates r_t , which define the links infectivity, and disease parameters. The strong underlying connectivity increases reachability among individuals [23,35]. Hence, the disease reaches the high degree individuals faster as r_t increases. Thus, there is a threshold value of r_t to grow disease prevalence I_p in the SPDT model. The threshold r_t reduces in the networks with high link density and for strong disease parameters.

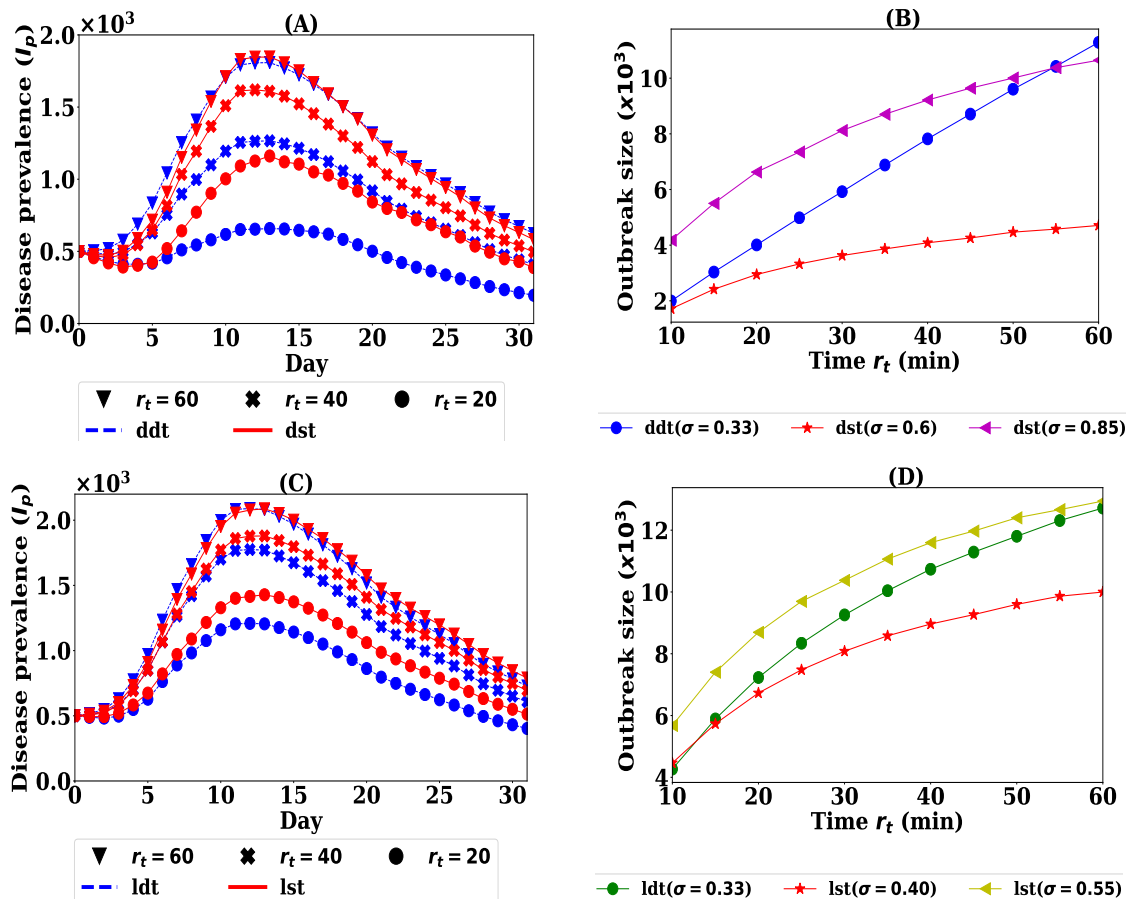


Figure 8. Reconstructing SPDT diffusion dynamics by SPST model and their differences over various particle decay rates r_t : A) comparing SPDT diffusion with $\sigma = 0.33$ and SPST diffusion with $\sigma = 0.85$, B) comparing outbreak sizes of SPDT model with $\sigma = 0.33$ and that of SPST model with $\sigma = 0.60$ and $\sigma = 0.85$, C) comparing LDT diffusion with $\sigma = 0.33$ and LST diffusion with $\sigma = 0.55$, and D) comparing outbreak sizes of LDT model with $\sigma = 0.33$ and that of LST model with $\sigma = 0.55$ and $\sigma = 0.40$

The SPDT model can capture realistic interactions for some diseases producing effective disease reproduction number R_e greater than one and making significant outbreaks while the SPST model could not produce R_e at any conditions. This shows the SPDT model based on indirect links is more realistic than the SPST model based on the direct links. The study of [44] on the real influenza outbreaks in various regions shows that the effective disease reproduction number will be in the range [1.06-3.0]. The SPDT model attains realistic disease reproduction number R_e having some values in this range at some values of r_t while the SPST model could not achieve realistic R_e for any r_t in our simulations. This quantitative assessment also shows the ability of SPDT model to capture realistic disease dynamics. The SPDT diffusion model can be applied to study influenza seasonality through modelling the particle decay rates r_t which can be varied over time with the fluctuations in the weather factors such as humidity and temperature [45,46].

5.2 New diffusion dynamics of SPDT

The SPDT model introduces novel diffusion behaviours that are not observed in SPST diffusion model. The underlying network connectivity in the SPDT model is changed with the particle decay rates r_t . The impact of this property on diffusion dynamics are not reproducible by the SPST model. This is observed by reconstructing equivalent SPDT diffusion dynamics for $\sigma = 0.33$ on the corresponding SPST network with strong σ (Fig. 8A and Fig. 8B). With $\sigma = 0.85$, the SPST diffusion dynamics become similar to that of SPDT model at $r_t = 60$ min (Fig. 8A) and outbreak sizes in both models are close to each other (Fig. 8B). However, diffusion dynamics and outbreak sizes in the SPST model are overestimated when r_t is lowered at $\sigma = 0.85$. On the other hand, the SPST model with $\sigma = 0.6$ shows the same total infections of SPDT model at $r_t = 10$ min but underestimates at the higher values of r_t . This is because the underlying connectivity in SPST model does not vary with changing r_t and spreading dynamic variations are limited.

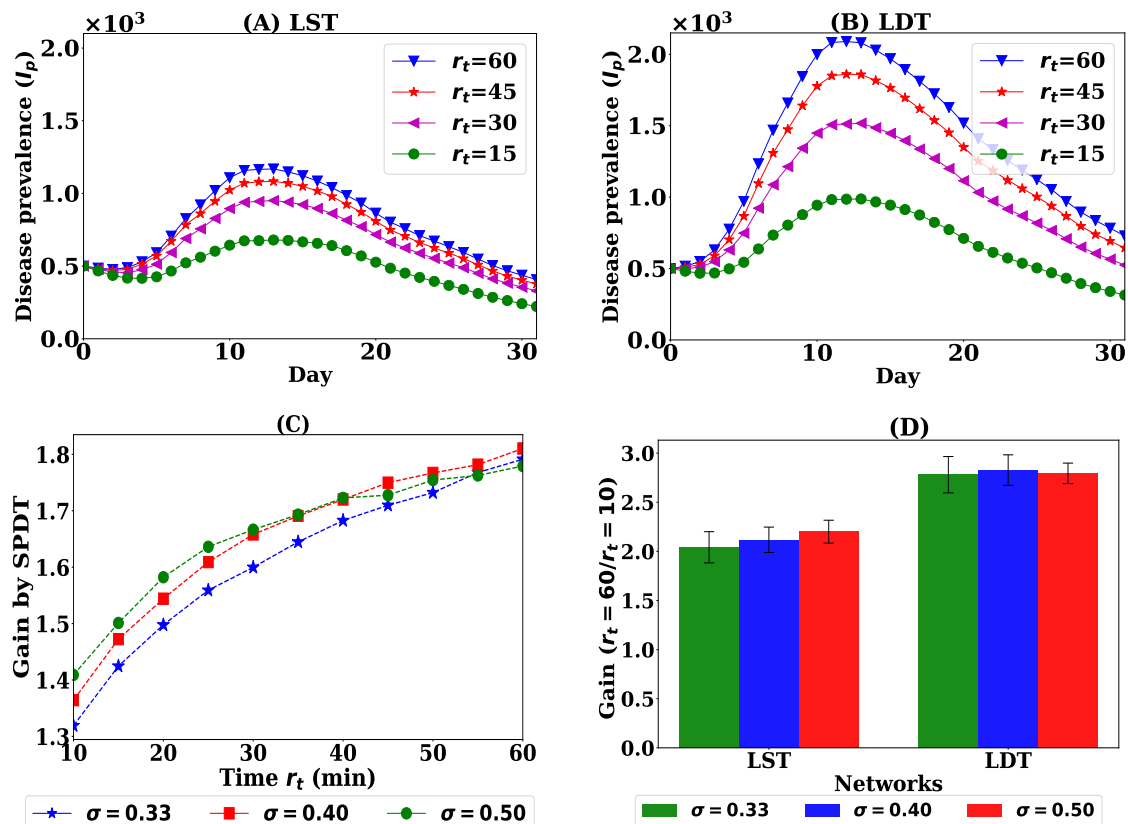


Figure 9. Diffusion on SPST and SPDT networks with controlled links densities: A) diffusion dynamics on LST network at $\sigma = 0.33$ varying r_t , B) diffusion dynamics on LDT network at $\sigma = 0.33$ varying r_t , C) gain by SPDT model over SPST model (LDT/LST) at various σ when both have same link densities, and D) infection gains for changing $r_t = 10$ min to $r_t = 60$ min at various σ

We also find the indirect transmission links significantly increase diffusion dynamics even if the underlying connectivity in the SPST and SPDT model is made the same. This is observed from the diffusion dynamics on the LST and LDT networks which maintain the same number of active users (having links every day) and the same link densities. Besides, the LDT network can be described such that some direct links of the LST network are appended with indirect links to generate it. Therefore, the underlying connectivity is not changed with r_t , but the links get stronger with increasing r_t . The LDT network still shows significantly stronger disease prevalence relative to LST network (Fig. 9A and Fig. 9B). By including indirect links, the LDT network achieves a strong disease reproduction rate R and produces a high disease prevalence I_p .

Our experiments also show that indirect transmission links are more affected by r_t compared to direct links. This phenomenon is also not reproducible by the SPST model which is observed reconstructing LDT diffusion dynamics on the LST network with increasing σ (Fig. 8C and Fig. 8D). With $\sigma = 0.55$, the LST diffusion dynamics become similar to the LDT diffusion and causes same number of infections at $r_t = 60$ min. However, the diffusion dynamics and outbreak sizes are overestimated at low r_t . In contrast, LST network with $\sigma = 0.4$ shows same outbreak sizes of LDT network at $r_t = 10$ min but underestimates at higher values of r_t . This difference is happening because the indirect link propensity is more sensitive to r_t than direct links. However, the variations in the reconstructed LST diffusion is small comparing to the DST network as the underlying connectivity is diminished in LDT network.

The SPDT model assumes longer linear amplifications of infections with r_t . We have seen the growth in SPDT amplification increases at high r_t as σ increases while it drops in SPST network (Fig. 7). The underlying cause is found studying diffusion on LST and LDT networks for $\sigma = \{0.33, 0.4, 0.5\}$ (Fig. 9C and Fig. 9D). Unlike the previous diffusion dynamics (Fig. 7), the gain across r_t (total infections at $r_t = 60$ /total infections at $r_t = 10$) slightly drops in LDT network which is the behavior of SPST model where the growth in amplification at low r_t is more than that at high r_t when σ increases. Due to having strong R for indirect links, the infection force in LDT network overrides infection resistance force at $\sigma = 0.4$, but it is affected at $\sigma = 0.5$. The LDT network gain reaches a steady state which did not happen in the DST network. Thus, the SPDT model with underlying network dynamics supports extended spreading opportunities.

5.3 Limitations

The applied individual contact networks are built among the Momo users and the contacts of Momo users with other individuals are not included in our simulations. In addition, the networks do not include the contacts while users are not using the App. Therefore, some potential transmission links could be missed and outbreak sizes could be different. With the known sparse contact data, we reconstructed the denser versions of empirical network repeating the available links for the missing days. This process has the following limitations: 1) limited link variation. When a user is present in the network for one day with only one indirect link, this indirect link is repeated for the missing 31 other days. This can not capture link variations for this user in reality, and 2) limited contact neighbours. When a user only presents one day, the same links are repeated for all missing days with the same old neighbours and new neighbours are not included. Thus, the disease spreading may be underestimated due to these limitations. Despite these issues, the MoMo dataset provides a city-scale population dataset with high position resolution (compared to cellular call data records [40,47] for instance), and therefore capture population movements and contacts at the sufficiently accurate resolution to drive useful observations on the spreading dynamics.

We have used a simplified infection risk assessment model where links between two individuals are created if they are within 20m of each other based on the GPS locations. However, the collected GPS locations may have errors when phones use Cell-ID or Wi-Fi signal for estimating GPS locations [48]. Thus, the individuals beyond 20m distance might have created links in our developed networks and thus overestimation can occur. In the calculation of exposures, particles concentration decay over distance from an infected individual is neglected. The infection risk model is assigned random particles decay rates picking up from a range to mimic the heterogeneity of interaction locations due to architecture, wind-flow, humidity and temperate variations. However, this variation is not fitted with real-world data. We also avoid the heterogeneity of individuals in infectious particle generation, particles inhalation and susceptibility to disease.

5.4 Future works

The SPDT diffusion dynamics are highly influenced by the individual level-interaction data that is difficult to obtain from real scenarios. Thus, it would be interesting to develop synthetic networks capturing the properties of real contact traces. In this study, we have only studied the overall diffusion dynamics on the contact networks. The indirect

transmission links may change local contact structure and hence disease emergence conditions can be altered in SPDT model. This would be an interesting research direction to assess the potential of indirect links in emerging diseases. As the inclusion of indirect links makes one individual connect with others, the probability of being super-spreader increases. Thus, an important research direction is to find the vaccination strategies for SPDT model. The individual-level contact mechanisms also influence the higher order network properties. It would be interesting to know how the modified higher order networks properties with indirect links influence the diffusion dynamics. Contact generalizations and finding the relationship between them and the total epidemic size is an interesting research direction for future work. We have assumed that the infectious particles can travel up to 20m in horizontal distance. It would be interesting to know to what extent the diffusion dynamics are varied in our model compared to metapopulation modelling approaches, in which locations (households, schools, communities) are captured with systems of equations and the underlying network structure describes movements of contacts between communities.

References

1. S. Bansal *et al.*, "The dynamic nature of contact networks in infectious disease epidemiology," *J. Biol. Dyn.* 4(5), 2010.
2. J. Stehlé *et al.*, "Simulation of an seir infectious disease model on the dynamic contact network of conference attendees," *BMC Med.* 9(1), 2011.
3. D. J. Toth *et al.*, "The role of heterogeneity in contact timing and duration in network models of influenza spread in schools," *J. R. Soc. Int.* 12(108), 2015.
4. C. Huang *et al.*, "Insights into the transmission of respiratory infectious diseases through empirical human contact networks," *Sci. Rep.* 6, 2016.
5. A. Fernstrom and M. Goldblatt, "Aerobiology and its role in the transmission of infectious diseases," *Journal of pathogens*, 2013.
6. A. B. Bloch *et al.*, "Measles outbreak in a pediatric practice: airborne transmission in an office setting," *Pediatrics*, 75(4), 1985.
7. M. Shahzamal *et al.*, "Delay tolerant based warning message broadcasting system for marine fisheries," 2015.
8. M. Shahzamal and M. F. Pervez, "Smartphones based warning messaging system for marine fisheries and its characteristics," in *2016 International Conference on Informatics, Electronics and Vision (ICIEV)*. IEEE, 2016, pp. 111–116.
9. P. Jacquet, B. Mans, and G. Rodolakis, "Information propagation speed in mobile and delay tolerant networks," *IEEE Transactions on Information Theory*, vol. 56, no. 10, pp. 5001–5015, 2010.
10. E. Bakshy, I. Rosenn, C. Marlow, and L. Adamic, "The role of social networks in information diffusion," in *Proceedings of the 21st international conference on World Wide Web*. ACM, 2012, pp. 519–528.
11. J. N. Wasserheit and S. O. Aral, "The dynamic topology of sexually transmitted disease epidemics: implications for prevention strategies," *Journal of Infectious Diseases*, vol. 174, no. Supplement_2, pp. S201–S213, 1996.
12. G. Sze To *et al.*, "Review and comparison between the wells–riley and dose-response approaches to risk assessment of infectious respiratory diseases," *Indoor Air*, 20(1), 2010.
13. M. Shahzamal, R. Jurdak, R. Arablouei, M. Kim, K. Thilakarathna, and B. Mans, "Airborne disease propagation on large scale social contact networks," in *Proceedings of the 2nd International Workshop on Social Sensing*. ACM, 2017, pp. 35–40.
14. D. Gruhl *et al.*, "Information diffusion through blogspace," in *Pro. 13th Int. Con. on WWW*, 2004.
15. S. Gao, J. Ma, and Z. Chen, "Modeling and predicting retweeting dynamics on microblogging platforms," in *Proceedings of the Eighth ACM International Conference on Web Search and Data Mining*. ACM, 2015, pp. 107–116.
16. T. O. Richardson *et al.*, "Beyond contact-based transmission networks: the role of spatial coincidence," *J. R. Soc. Int.* 12(111), 2015.
17. C. M. Issarow *et al.*, "Modelling the risk of airborne infectious disease using exhaled air," *J. The. Biol.* 372, 2015.
18. M. Shahzamal, R. Jurdak, B. Mans, and F. de Hoog, "A graph model with indirect co-location links," in *Proceedings of Workshop on Mining and Learning with Graphs (MLG)*, 2018.
19. C. J. Noakes *et al.*, "Mathematical models for assessing the role of airflow on the risk of airborne infection in hospital wards," *J. R. Soc. Int.* 6(6), 2009.
20. K. Thilakarathna *et al.*, "A deep dive into location-based communities in social discovery networks," *Comp. Com.*, 2016.
21. L. J. Allen *et al.*, *Mathematical epidemiology, 1945*. Springer, 2008.
22. M. Génois *et al.*, "Compensating for population sampling in simulations of epidemic spread on temporal contact networks," *Nat. Com.* 6, 2015.
23. P. C. Lopes *et al.*, "Infection-induced behavioural changes reduce connectivity and the potential for disease spread in wild mice contact networks," *Sci. Rep.* 6, 2016.
24. D. Rey *et al.*, "Finding outbreak trees in networks with limited information," *Net. and Spa. Eco.* 16(2), 2016.
25. A. RH *et al.*, "Human influenza resulting from aerosol inhalation," *Pro. Soc. for Exp. Biol. and Med.* 122(3), 1966.
26. J. Yan *et al.*, "Infectious virus in exhaled breath of symptomatic seasonal influenza cases from a college community," *Pro. Nat. Aca. of Sci.*, 2018.
27. W. G. Lindsley, *et al.*, "Viable influenza a virus in airborne

- particles from human coughs," *J. Occ. and Env. Hyg.* 12(2), 2015.
28. C. He *et al.*, "Particle deposition rates in residential houses," *Atm. Env.* 39(21), 2005.
 29. E. Riley *et al.*, "Airborne spread of measles in a suburban elementary school," *Am. J. Epi.* 107(5), 1978.
 30. G. N. Sze-To *et al.*, "Effects of surface material, ventilation, and human behavior on indirect contact transmission risk of respiratory infection," *Risk Analysis*, 34(5), 2014.
 31. Z. Han *et al.*, "A risk estimation method for airborne infectious diseases based on aerosol transmission in indoor environment," in *Pro. W. Cong. on Eng.* 2, 2014.
 32. C. Howard-Reed *et al.*, "The effect of opening windows on air change rates in two homes," *J. Air & Waste Man. Asso.* 52(2), 2002.
 33. S. Shi *et al.*, "Air infiltration rate distributions of residences in beijing," *Build. and Env.* 92, 2015.
 34. G. Chowell, S. Echevarría-Zuno, C. Viboud, L. Simonsen, J. Tamerius, M. A. Miller, and V. H. Borja-Aburto, "Characterizing the epidemiology of the 2009 influenza a/h1n1 pandemic in mexico," *PLoS Med*, vol. 8, no. 5, p. e1000436, 2011.
 35. M. D. Shirley *et al.*, "The impacts of network topology on disease spread," 2005.
 36. A. Hagberg *et al.*, "Exploring network structure, dynamics, and function using networkx," LANL, Los Alamos, USA), Tech. Rep., 2008.
 37. R. M. May *et al.*, "Infection dynamics on scale-free networks," *Phy. Rev. E* 64(6), 2001.
 38. M. Shahzamal *et al.*, "Electronic supplementary materials: Diffusion dynamics with collocation indirect interactions," 2018.
 39. S. T. Stoddard *et al.*, "The role of human movement in the transmission of vector-borne pathogens," *PLoS Neg Trop. Dis.* 3(7), 2009.
 40. A. J. Tatem *et al.*, "Integrating rapid risk mapping and mobile phone call record data for strategic malaria elimination planning," *J. Malaria*, 13(1), 2014.
 41. M. L. Brennan *et al.*, "Direct and indirect contacts between cattle farms in north-west england," *Pre. Vet. Med.* 84, 2008.
 42. M. Lange *et al.*, "Relevance of indirect transmission for wildlife disease surveillance," *Front. in Vet. Sci.* 3, 2016.
 43. S. A. Boone *et al.*, "Significance of fomites in the spread of respiratory and enteric viral disease," *App. and Env. Microb.* 73(6), 2007.
 44. M. Biggerstaff *et al.*, "Estimates of the reproduction number for seasonal, pandemic, and zoonotic influenza: a systematic review of the literature," *BMC Inf. Dis.* 14(1), 2014.
 45. A. C. Lowen and J. Steel, "Roles of humidity and temperature in shaping influenza seasonality," *Journal of virology*, vol. 88, no. 14, pp. 7692–7695, 2014.
 46. A. I. Barreca and J. P. Shimshack, "Absolute humidity, temperature, and influenza mortality: 30 years of county-level evidence from the united states," *American journal of epidemiology*, vol. 176, no. suppl_7, pp. S114–S122, 2012.
 47. J. Candia *et al.*, "Uncovering individual and collective human dynamics from mobile phone records," *J. Phy. A: Mat. and The.* 41(22), 2008.
 48. P. A. Zandbergen, "Accuracy of iphone locations: A comparison of assisted gps, wifi and cellular positioning," *Tran. in GIS*, 13, 2009.